RIO 2005 inter-noise ENVIRONMENTAL NOISE CONTROL
The 2005 Congress and Exposition on Noise Control Engineering
07-10 August 2005 - Rio de Janeiro - Brazil

Random Thinning of Segmented Annular Arrrays

G. Godoy[a], O. Martínez[b], A. Ibañez[b], L.G. Ullate[b]

[a]E.U.P. de Linares, Universidad de Jaén, 23700 Linares - Jaén, Spain
[b]Instituto de Automática Industrial-CSIC, La Poveda, 28500,Arganda del Rey-Madrid, Spain
[a]ggodoy@ujaen.es; [b]oscarm@iai.csic.es; [b]aibañez@iai.csic.es; [b]luisg@iai.csic.es

Abstract Nowadays, two-dimensional (2D) arrays design is base in a square matrix (SM) distribution of elements, which requires a pitch of λ/2 in order to eliminate grating lobes. From this condition, a 2D array will contain between 1500 and 16000 elements, which are much higher than the number of channels of present image systems. A well-known technique for reducing the number of active elements is based on randomly eliminating a part of the elements from the aperture. Segmented-annular (SA) arrays constitute an alternative to SM arrays for the generation of volumetric images, because they have lower periodicity than squared patterns, and therefore they allow increasing the inter-element distance up to λ or even further. SA arrays, then, the number of elements are divided by four with respect to SM arrays using the full aperture. However, this number is still a challenge for the existent technology, so requiring thinning the aperture. In this work, a thinning technique based on random sparse is applied to segmented-annular arrays and squared-matrix arrays. Several random layouts are applied to equivalent SM and SA arrays (equivalent arrays have the same active area and the same number of elements, which are of similar size and aspect ratio), and the comparative results are then theoretically analyzed in the paper.

1. INTRODUCTION

Typical two-dimensional (2-D) arrays distribute their elements in the cells of a square matrix (SM), Figure 1 (a). Due to regularity of the aperture, the interelement spacing must be maintained below half wavelength (λ) in order to avoid the grating appearing at the array main directions [1]. Three main drawbacks are derived from this condition which make difficult the use of 2-D arrays in commercial applications: the number of elements is very high in relation to the present technological level, the complexity of the inter-connections and finally, as the elements are so small, the electrical impedance is too high, causing a very low signal to noise ratio in the images.

In order to reduce the number of elements several methods have been proposed [1] [2] [3]. Some of them are based on random dispersed openings [1] (by means of a random selection of the active elements); a second method uses different complementary apertures in emission

and reception in order to reduce the grating lobes. The vernier aperture [4] [5] is a good example of this method, producing good image resolution with reducing factors over one order of magnitude. However, these two solutions require maintaining the interelement distance below λ/2, and therefore, the field intensity is reduced drastically, and consequently, the signal to noise ratio of the images.

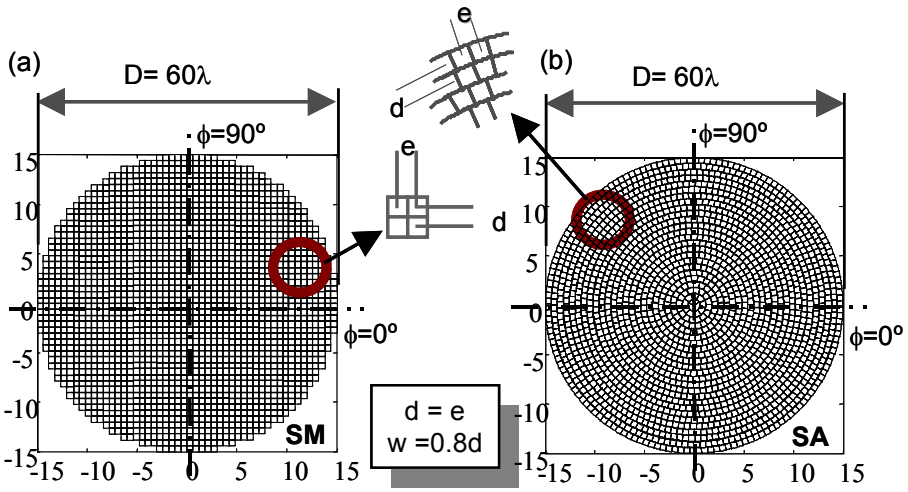

Figure 1. Geometry of the equivalent arrays SM (a) and SA (b) (D=60λ, d=1.2λ).

An alternative method uses curvilinear arrays, which have more spatial diversity, and therefore allow surpassing the λ/2 constraint associated to SM arrays [11]. In several works [10] [12], we have proposed using segmented annular (SA) figure 1 (b) which have elements of equal size distributed in the rings of a circular aperture. SA arrays are a good alternative to SM arrays, as they allow increasing the inter-element distance up to 1,2λ holding, at the same time, full aperture conditions [12]. Although this means a reduction of the number of elements by 6, the complexity can still be too high for nowadays imaging systems (e.g.: for an array with diameter D=60λ, the number of elements is 1960). In this case, thinning techniques can be applied to SA arrays in order to reduce the number of elements.

In this work, thinning techniques based on a random removal of active elements are applied to SA and SM arrays of equivalent geometry and number of elements. The comparisons are made for both: the *array factor*, which considers the array formed by point like sources emitting continuous wave, and a more realistic array with the *real size of elements* and wide band pulses.

2. COMPUTING METHOD

For simulations we assume a 2-D array of diameter D lying in the Z=0 plane of a Cartesian coordinates system. The N elements of the array vibrate like a piston with a velocity *v(t)*. The array emits ultrasonic waves, which propagate with a velocity *c* through a homogeneous liquid medium of density ρ_0. Infinitely rigid baffle is assumed for boundary conditions. The pressure waveform p(·) radiated over a field point $\bar{x}$ is obtained by superposition:

$$p(\bar{x},t)=\rho_0\frac{dv(t)}{dt}*\sum_{i=1}^{N}h_i(\bar{x},t-T_i^F)=\rho_0\frac{dv(t)}{dt}*h_A(\bar{x},t)\rightarrow i=1:N \tag{1}$$

Where $h_A(\cdot)$ is the velocity potential impulse response of the array, $h_i(\cdot)$ is the impulse response of the i^{th} array element located at $\bar{x}_i$, (*) indicates temporal convolution, and T_i^F are the time delays for focusing the beam at the point $\bar{x}^F$:

$$cT_i^F=\left|\bar{x}^F-\bar{x}_i\right|-\left|\bar{x}^F\right| \tag{2}$$

The transmit-receive mode is simulated considering that the received signal s(t) due to a point target at $\bar{x}$ is given by:

$$s(\bar{x},t)=\frac{\rho_0}{c}\frac{\partial^2 v(t)}{\partial t^2}*\left\{h_A^T(\bar{x},t)*h_A^R(\bar{x},t)\right\} \tag{3}$$

where $h_A^T(\cdot)$ and $h_A^R(\cdot)$ are the emit and receive spatial impulse responses of the array.

The impulse response of the array elements can be calculated in the time domain by direct computation, dividing the array into squared cells of elementary area [6]. If the surface of the i^{th} element is separated into N_i squared cells of elementary area ΔS, the velocity potential impulse response becomes the sum:

$$h_i^*(\bar{x},t)=\sum_{j=1}^{N_i}\frac{\delta(t-r_j/c)}{2\pi r_j}\Delta S \tag{4}$$

where r_j is the distance from the j^{th} cell to the field point $\bar{x}$, and h_i^* means the discrete representation of the impulse response. In computations, the elementary cells are taken $\lambda/5*\lambda/5$ of size and the sampling time is $\Delta t=\lambda/64c$. The computation error in these conditions is below 2% for every point in the field of interest [10].

When the array elements are assumed as point sources, the ultrasonic field is calculated from equations (3) and (4), considering single cells at the center of the array elements, with weight equal to the element area.

3. ARRAY CONFIGURATIONS

All simulations are based on the two apertures (SA1 and SM1) shown in figure 1, which are of equivalent characteristics: their diameter is $D=60\lambda$, their interelement distance is $d=1.2\lambda$, and both have 1964 elements with unitary aspect ratio. From these basic apertures, we shall analyse the response of thinned apertures following two ways for selecting the array active elements: *ramdom arrays* (a) and *binned arrays* (b), and in both cases we shall also try aperture designs with no common elements between the emitting and the receiving apertures. We consider the reduction order p as the ratio between the array active elements Nr in emission or reception, and the number of elements N of the full aperture: p=Nr/N. In the *random aperture*, the Nr active elements are selected following a probabilistic distribution [7], while in the *binned arrays*, the array is divided into Nr equal-sized bins, and an element is chosen at random within each bin. *Random non-overlapping* transmit and receive layouts

can be interesting for certain image systems, where the receiving circuits are of low voltage. In this case, the receiving elements are randomly selected avoiding the coincidence with the emitting ones. We shall choose the same number of elements Nr in emission and in reception. From the different random distributions that can be used (uniform [1], Gaussian [8], triangular [9], etc. we shall take only the uniform distribution in our simulations.

4. COMPARATIVE ANALYSIS USING THE ARRAY FACTOR IN TWO-WAYS MODE

Figure 2 shows a 3D representation of the pulse-echo field of SM1 and SA1 for different emission/reception apertures, considering the array factor case. The full array is shown in parts (a) and (d) of the figure, and shows how SM1 has a field with high peaks due to grating lobes (GL) in the array main directions, while SA1 presents a field where the grating lobes expand over an annular zone around the main lobe. In Figure 3 (a), the quantitative values of the grating lobes can be observed: while SM1 generates grating lobes located at $\theta=\pm 57º$, which are as high as the main lobe, in the SA1 case, the GL level is around 40 dB below the main lobe. This is due to the lower periodicity of the sectorial aperture with respect the square matrix.

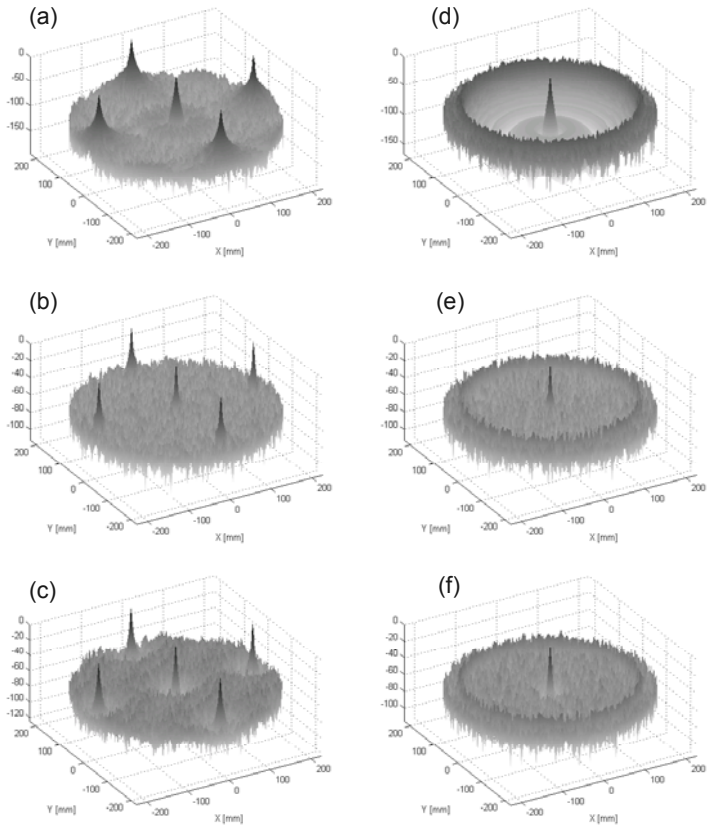

Figure 2. 3D representation of the beam pattern in pulse-echo mode (the array factor considers that the array elements are points vibrating in continuous wave): (a) full SA array and (d) full SM array. For p=4 random thinning: (b) SM array and (e) SM array. (c) and (f) idem for p=4 binned random thinning.

The case of random thinning with a reduction order of p=4 is shown in figures 2(b, e) and 3(b), where the number of active elements has been reduced from 1964 to N_E=N_R=491. We can observe that for both arrays, in the one hand, the grating lobes are located at the same place and have the same relative level than the full array but, on the other hand, the resting secondary lobes (SL) form a pedestal whose mean level in the pulse-echo case is:

$$P(pedestal) \approx 20\log\left(\frac{1}{\sqrt{N_E N_R}}\right) = 20\log\left(\frac{1}{Nr}\right) \tag{6}$$

This means that for N_E=N_R=491, the pedestal is at -54dB, which is coincident with the level shown in figure 3(b).

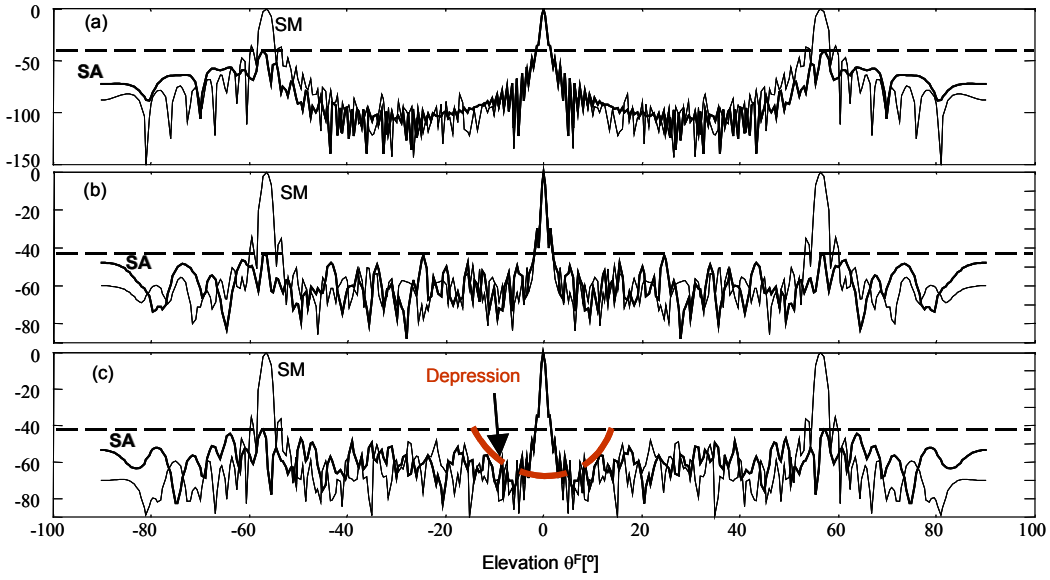

Figure 3. (a) Pulse-echo beam pattern at the azimut direction ϕ=0º, corresponding to the SM and SA arrays in the case of full array. (b) Idem for random thinning p=4. (d) Idem for binned random thinning p=4

The ultrasonic beam pattern of the binned array with factor reduction of p=4 is shown in the figures 2(c) and 3(c). This array has the characteristic that the side lobes around the main lobe decrease [9], although the main value of secondary lobes is maintained at the same value of the corresponding random aperture. The depression around the main lobe and the grating lobes of the SM array can clearly be seen in the figure 2(c). The segmented annular array with binned reduction also gives a depression around the main lobe, but the grating lobes are not modified presenting the annular form as the other cases shown in the figure 2.

We have also studied what is the effect of varying the number of common elements in both the emitting and the receiving apertures, with the following results in the secondary lobes: (a) the mean level of SL is maintained almost constant when the number of coincident elements in both apertures is kept low, but the SL level increases around 2dB when both apertures are coincident.

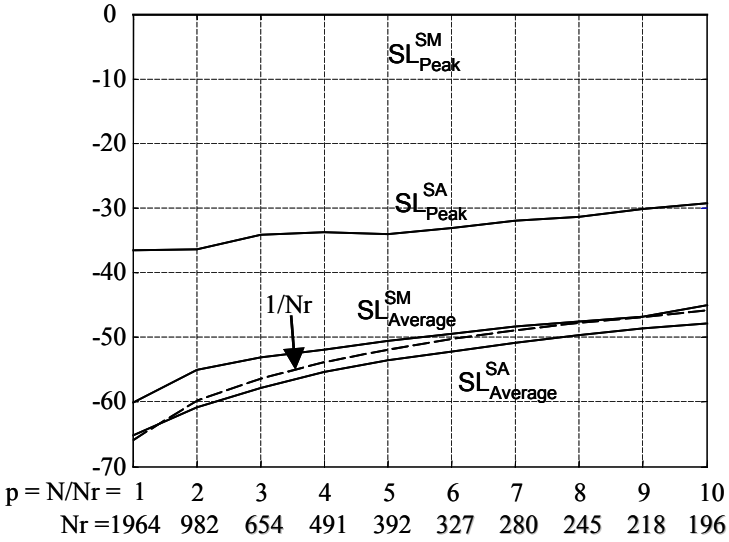

Figure 4. Array factor of SM1and SA1 (two-ways response): SL peak and SL average varying the factor reduction of the tinned aperture.

From figure 4, the influence of the reduction order p on the level of secondary lobes can be observed. With respect to the SL average, both the SM and SA arrays practically follow the curve given by equation (6), but the SA array keeps its level two or three dB below the equivalent SM array. With respect to the grating lobe peak, for every p, the SM array has its maximum at the same level as the main lobe, while the SA array produces its maximum in the range of -40dB and -30dB, increasing this value as the number of elements is reduced.

5. EFFECT OF FINITE SIZE OF ELEMENTS ON THE ARRAY BEAMFORMING

Our simulations in this epigraph have been made in pulse-echo mode, focusing the arrays SM1 and SA1 at the point F ($R^F=D^2/8\lambda$, $\theta^F=30º$, $\phi^F=0º$). A wide pulse with central frequency of 3MHz and 50% of bandwidth is used for excitation. The transducer emits into water, giving a wavelength of approximately 0.5mm.

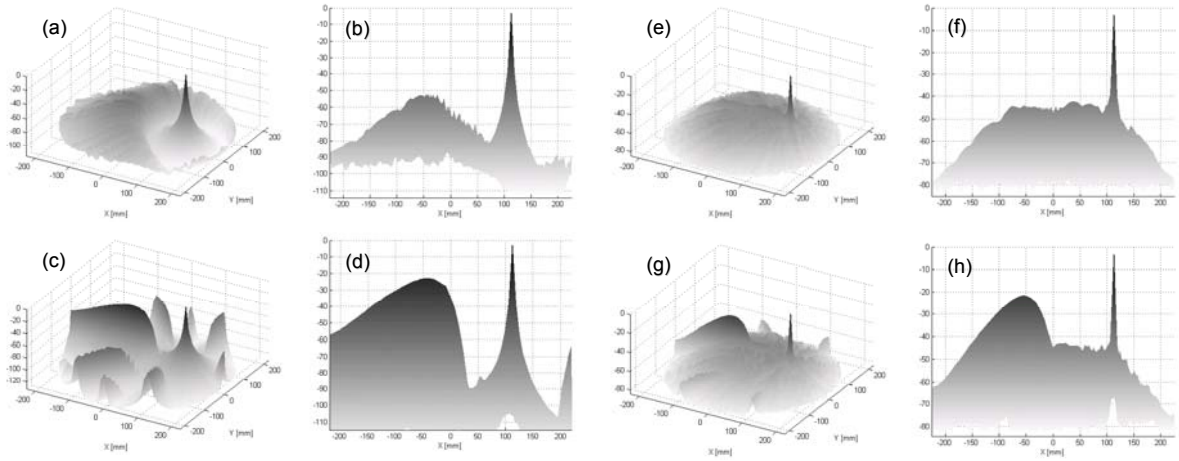

Figure 5. Wide-band beam patterns of SA1 (top) and SM1 (button) considering the real size of elements (w=0.8d). 3D representation of the focal hemisphere in pulse-echo focusing at $D^2/8\lambda$, $\theta^F=30º$, $\phi^F=0º$. (a), (b), (c) and (d) are for the full array, (e), (f), (g) and (h) are for the random thinning with p=9. (b), (d), (f) and (h) represent projections on the y=0 plane.

On the one hand, the main beam resolution corresponding to the thinned array is very similar to the full array case, presenting in both cases an angular beam-width of 1.7º and 4.7º at levels of -20dB and -40dB respectively. The SL pedestal, on the other hand, is modulated by the element factor showing a convex response with a drop of amplitude in the zone where the elevation angle θ is higher (Figure 5). The maximum and average of the SL zone is a function of several parameters, e.g.: the number of elements, pulse bandwidth, steering angle, etc. In table 1, the influence of the pulse bandwidth on the SL peak and SL average is shown for a random reduction of p=9: an improvement of 10 dB is obtained from continuous wave to wide band pulses.

Table 1: SA1 array: peak level (SL_{Peak}) and average ($SL_{Average}$) of the SL region, varying the bandwidth B relative to the central frequency of the ultrasonic pulse. The factor reduction is p=9, and the array has been focused at F ($D^2/8\lambda$, $\theta^F=0º$, $\phi^F=0º$).

B (%)	SL_{Peak}	$SL_{Average}$
0	-39.5	-65.0
25	-44.9	-69.2
50	-47.2	-71.7
75	-47.2	-73.0
100	-50.3	-74.4

Due to the finite size of the elements, in the order of λ for the examples, the steering angle θ^F causes an increase of the secondary lobes. Figure 6 shows the values of SL peak and SL average with and without steering for different reduction orders. Comparing the array types, the figure shows that SA1 produces SL levels that are below SM1, this difference is greater when the steering angle increases, but it is reduced when the reduction order increases. The SL peak and SL average curves of SA1 are affected by the number of active elements and, in fact, they approximately follow the 1/Nr curve at different levels, which are determined by the element size, the pulse bandwidth and the steering angle.

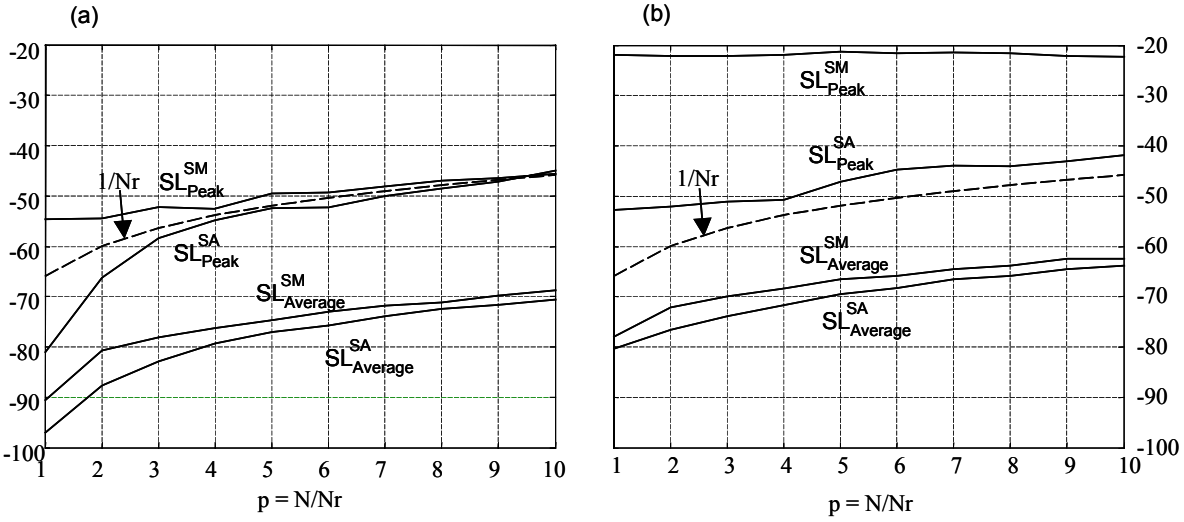

Figure 6. Two-ways response of SM1 and SA1 (real size) in wide band: SL_{Peak} and $SL_{Average}$ varying the reduction factor of the random thinned arrays: (a) No steering, $\theta^F=0º$, (b) $\theta^F=30º$.

Finally, if we apply to SA1 values of p up to 4, the SL peak will be below -50dB and the SL average below -70 dB, being both values acceptable for ultrasonic image applications. The array in this case will have 490 active elements, and 25% of active area. This is in contrast with the typical design of a SM array with $\lambda/2$ interelement spacing, that needs a reduction order of 30 for holding 490 active elements, and the active area would be 3% of the full array.

6. CONCLUSION

In this paper, a thinning method based on the random selection of the active elements of a 2D annular segmented array has been analysed based on two different approaches: the Array Factor, which considers omni-directional elements vibrating in continuous wave, and the real aperture in wide band. Moreover, a comparison with the conventional squared matrix array of equivalent characteristics has also been included, obtaining the following conclusions:

- The array factor shows that the effect of random thinning preserves the beam characteristics of the full array in both array types (main lobe and grating lobes are coincident) but the secondary lobes are spread on a platform whose height is inversely proportional to the number of active elements of the aperture.

- Simulations considering the real geometry of the aperture and wide band pulses show SL levels improving with several factors, such as increasing the number of active elements, increasing the wide band, or decreasing the steering angle.

Finally, it is shown that a SA array with $D=60\lambda$, interelement spacing $d=1.2\lambda$ and element size $e=\lambda$, using 490 active elements, produces side lobes with de peak at -50dB with respect the main lobe, and the SL average at -70 dB, being both values acceptable for ultrasonic image applications. The array active area will be in this case 25% of the full array. This is in contrast with the typical design of a SM array with $\lambda/2$ interelement spacing, that needs a reduction order of 30 for holding the same number of active elements, and the active area would be reduced to 3% of the full array.

7. ACKNOWLEDGEMENTS

This paper received the support of the Education and Science Ministry of Spain under its DPI2002-01583, DPI2004-06470 and DPI2004-06756 projects.

REFERENCES

[1] D. H. Turnbull and F. S. Foster, "Beam Steering with pulsed two-dimensional transducer arrays", *IEEE Trans. on Ultrason., Ferroelec. and Freq. Control*, vol. 38, no. 4, pp. 320-333, 1991

[2] Jesse T. Yen, Jordan P. Steinberg and S. W. Smith, "Sparse 2-D array design for real time rectilinear volumetric imaging", *IEEE Trans. on Ultrason., Ferroelec. and Freq. Control*, vol. 47, no. 1, pp. 93-110, 2000

[3] Andreas Austeng and Sverre Holm, “Sparse 2-D arrays for 3-D phased array imaging: Design methods”, *IEEE Trans. on Ultrason., Ferroelec. and Freq. Control*, vol. 49, no. 8, pp. 1073-1086, 2002

[4] S. S. Brunke and G. R. Lockwood, “Broad-bandwith radiation patterns of sparse two-dimensional vernier arrays”, *IEEE Trans. on Ultrason., Ferroelec. and Freq. Control*, vol. 44, no. 5, pp. 1101-1109, 1997

[5] G. R. Lockwood and F. S. Foster “Optimizing the radiation pattern of sparse periodic two-dimensional arrays”, *IEEE Trans. on Ultrason., Ferroelec. and Freq. Control*, vol. 43, no. 1, pp. 15-19, 1996

[6] B. Piwakowski and S. Khalid, “A new approach to calculate the field radiated from arbitrarily structured transducer arrays”, *IEEE Trans. on Ultrason., Ferroelec. and Freq. Control*, vol. 46, no. 2, pp. 422-440, 1999

[7] B. D. Steinberg, “Principles of aperture and array system design”, New York: Willey and Song, pp. 138-169, 1976

[8] R. E. Davidsen, J. A. Jensen and S. W. Smith, “Two-dimensinal random arrays for real time volumetric imaging”, *Ultrason.Imag.*, vol 16, pp. 143-163, Jul. 1994

[9] W. J. Hendricks, “The totally random versus de bin approach for random arrays”, *IEEE Trans. on Ultrason., Ferroelec. and Freq. Control*, vol. 39, no. 12, pp. 1757-1762, 1991

[10] G. Godoy, “Metodología de diseño de arrays bidimensionales de geometría anular para generación de imagen ultrasónica 3D”, *Ph. D. Thesis dissertation*, UNED, Madrid, 2004

[11] H.P. Schwartz and B.D. Steinberg, "Ultrasparse, ultrawideband arrays", *IEEE Trans. on UFFC*, 45 (2) , 376-393, 1998

[12] Luis G. Ullate, G. Godoy, O. Martínez, M.T. Sánchez, "Beam steering with segmented annular arrays”, IEEE Trans. on UFFC, pp. 1-28, (to be accepted)